RSC Advances

ROYAL SOCIETY OF CHEMISTRY

www.rsc.org/advances

Journal Name

RSCPublishing

ARTICLE

Cite this: DOI: 10.1039/x0xx00000x

Facile Synthesis of Hollow Hierarchical Ni/γ-Al_2O_3 Nanocomposites for Methane Dry Reforming Catalysis

Received 00th January 2012,
Accepted 00th January 2012

DOI: 10.1039/x0xx00000x

www.rsc.org/

Qing Zhang[1], Tao Wu[1], Peng Zhang[1], Ruijuan Qi[2], Rong Huang[2], Xuefeng Song[1], and Lian Gao[1]**

Hydrogen reduction of hierarchical spinel intermediates that were synthesized by a facile hydrothermal method results in Ni/γ-Al_2O_3 nanocomposites with Ni nanoparticles (~ 5.5 nm) well dispersed and embedded in nanoflakes of the hollow Al_2O_3 microspheres. The good dispersion of small metal nanoparticles and strong metal-support interaction that were resulted from decomposition of spinel intermediate during reduction are essential for the efficient and sustainable high temperature dry reforming of methane (DRM) catalysis. The high surface area (170 m^2/g) composite catalysts show coke and sintering resistance in long term DRM catalysis at 750 ^oC, the highest temperature ever tested for hierarchical nanostructures. Ni loadings and the calcination temperatures of the spinel intermediate are investigated for their effect on the morphology and the catalytic performance of the final catalysts. It is interesting that some initially none-active control catalysts can be activated during long term test.

Introduction

In the past centuries, the utilization of fossil fuels has allowed an unprecedented advancement of the society.[1,2] However, the consumption and mining of these nonrenewable energy resources emit a vast quantity of CO_2 and CH_4 into the atmosphere. Reducing the green house gases emission is vitally important and has become one of the most profound challenges of the 21st century.[3,4] In recent years, the catalytic dry reforming of methane has aroused more attention from both the economic and environmental standpoints.[5-14] This process provides an effective approach to convert two greenhouse gases (CH_4, CO_2) into syngas with a low H_2/CO molar ratio of ~1, which is more suitable for the production of oxygenated hydrocarbons and liquid fuels.[15-18] Moreover, It may also lead to more efficient utilization of CO_2-rich natural gas by reducing the cost for separating CO_2 from natural gas.[19]

It is well known that noble metals (Pt, Pd, Rh, *etc.*) exhibit superior catalytic performance for dry reforming of methane (DRM).[20-22] Considering the high cost and limited availability of the precious metals, they are not economically competitive in comparison with other transition metal based materials. Among the non-noble metals, supported Ni nanomaterials are the most promising catalysts for DRM due to their high activity, low cost, and extensive availability. However, the Ni catalysts suffered from rapid deactivation because of the carbon formation and the sintering of nickel particles.[23-27] Therefore, great efforts are still needed to develop efficient Ni catalyst with enhanced activity and stability for practical applications.

The most commonly used method to prepare Ni catalyst supported on oxides is the impregnation method. However, the resulted relatively weak metal-support interaction has weak resistance to metal particle sintering at high temperature, often resulting in rapid deactivation of catalysts.[28,29] In addition, the relatively large size of the metal particles (> 10 nm) is regarded as a reason for the coke formation due to the presence of rich surface terraces on large Ni ensembles.[28,30-31]

In searching for more robust DRM catalysts, researchers have developed various nanostructures for Ni based catalysts with a combination of excellent catalytic activity, selectivity, and good resistance to coke and sintering. The catalysts derived from layered double hydroxides (LDHs),[31-33] also known as hydrotalcite-like compounds containing both divalent and trivalent metal cations, are promising for DRM reaction. After high-temperature annealing, the ordered layer structure will transform into metal oxides owning large surface areas, high thermal stability, and strong metal-support interactions after hydrogen reduction. Zhang *et al*. recently prepared catalysts with supported hydrotalcite-like films on Al wires through in situ growth.[34] The strong metal-support interactions and the small sized Ni nanoparticles supported on MgO-Al_2O_3 resulted in significant reduction in coke formation and higher resistance to sintering in DRM reaction. Xue and coworkers successfully prepared a surface defect-promoted Ni nanocatalyst with good metal dispersion and high particle density on the Al_2O_3 matrix.[35] The sintering resistance property was attributed to the strong anchoring of Ni nanoparticles on the surface of the support. Besides the metal particle sizes and the metal-support interaction, the nature of the surface -OH groups on the catalyst surface also plays a significant role in the catalysis.[36]

The catalytic performances of nano/microstructured composite materials are strongly related to their structures and morphologies. It

is well established that small particle size with high surface area and accessible metal surface can effectively improve the catalytic performance.[35] Due to the large specific surface area and the easy access of reactant species to the catalytic sites, the oxides with hollow hierarchical macro-mesoporous structures are good candidates for catalyst supports.[37,38] Nie *et al*. reported rational design of Pt/hierarchical hollow Al_2O_3 through impregnation.[37] The catalyst displayed superior catalytic performance for oxidative decomposition of HCHO because of the high specific area and accessible open surface. Similar result was reported by Wang about Au/hollow γ-Al_2O_3 catalyst for CO oxidation.[38] All these reactions were operated at low temperatures (<100 °C), where the weak metal-support interaction resulted from impregnation method is not a big problem. The applications of hollow hierarchical catalysts at high temperatures (*e.g.* >600 °C) have not been reported and therefore the thermostability of the hierarchical structures is unknown.

In this work, we use a facile method to fabricate nanocomposite catalysts with well dispersed Ni nanoparticles supported on hierarchical hollow γ-Al_2O_3 spheres (NAO) through in situ hydrothermal growth followed by high temperature calcination and hydrogen reduction. The obtained catalysts possess large surface area, high particle density, high catalytic activity, and high thermal stability in DRM catalysis. The results present a promising catalyst for chemical conversion of greenhouse gases into valuable chemicals.

Experimental Section

Materials: $Ni(NO_3)_2{\cdot}6H_2O$, $KAl(SO_4)_2{\cdot}12H_2O$ (alums), $CO(NH_2)_2$ (urea) and $AlCl_3{\cdot}6H_2O$ were obtained from Sinopharm Chemical Reagent Co. Ltd, China. The γ-Al_2O_3 was obtained from Aladdin Reagent Inc. All the reagents were used without additional purification.

Preparation of hierarchical NiAl-LDH precursors: Hierarchical NiAl-LDH precursors were synthesized through hydrothermal synthesis method. In a typical synthesis of NiAl-LDH, alums (0.8000 g) and urea (0.4000 g) was dissolved in an aqueous solution of $Ni(NO_3)_2{\cdot}6H_2O$ (0.1M, 8 ml, equivalently 0.2326 g) and deionized water (17 ml) under vigorous stirring for 30 minutes at room temperature. Then the solution (25 ml) was transferred into a 50-mL Teflon-lined autoclave and heated at 180 °C for 15 h. The resulting precipitates were separated by centrifugation and washed 3 times with deionized water, then dried at 60 °C for 4 hours. For the comparison of catalytic activity with different Ni loadings, a series of hierarchical NiAl-LDH precursors were synthesized using the same method, while the volume of $Ni(NO_3)_2{\cdot}6H_2O$ (0.1M) aqueous solution varies from 8 ml to 13 ml (equivalently 0.3780 g) and 20 ml (equivalently 0.5816 g) to have different loading amount of Ni.

Preparation of hierarchical NiO-γ-Al_2O_3 (NOAO) sphere: In a typical synthesis of NiO-γ-Al_2O_3, the dry powers of NiAl-LDH precursor were finely grounded in an agate mortar and calcined in air for 5 h at 800 °C. For the purpose of comparison, the NiAl-LDH precursors synthesized from 8 ml $Ni(NO_3)_2{\cdot}6H_2O$ (equivalently 0.2326 g) are also calcined at 400 °C and 600 °C.

Preparation of hollow hierarchical Ni-γ-Al_2O_3 (NAO) sphere: NOAO spheres with different Ni molar contents and calcination temperatures were reduced in 5% H_2/Ar (20 ml/min) for 2 h at 700 °C. The obtained products are hierarchical Ni/Al_2O_3 catalysts with theoretical Ni loadings of 35 wt%, 47 wt% and 58 wt%, and are denoted as NAO (35 wt%, 400 °C), NAO (35 wt%, 600 °C), NAO (35 wt%, 800 °C), NAO (47 wt%, 800 °C) and NAO (58 wt%, 800 °C), respectively for samples whose oxide precursors calcined at different temperatures. For comparison, Ni/Al_2O_3 nanosheet (35 wt%, 800 °C), IM-NAO (35 wt%, 800 °C) and IM-γ-Al_2O_3 (35 wt%, 800 °C) were synthesized using a similar method. In the synthesis of Ni/Al_2O_3 nanosheet (35 wt%, 800 °C), alums (0.80 g) were replaced with $AlCl_3{\cdot}6H_2O$ (0.407 g) in the hydrothermal reaction. In the synthesis of IM-NAO (35 wt%, 800 °C), the precursor was synthesized through impregnation. $Ni(NO_3)_2{\cdot}6H_2O$ solution (8 ml, 0.1M) was added into hollow AlOOH spheres (synthesized from hydrothermal method with 0.80 g alums and 0.40 g urea at 180 °C for 15 h) and the mixture was continually stirred for 10 h at room temperature. The IM-Ni/γ-Al_2O_3 (35 wt%, 800 °C) was obtained by impregnation of Ni^{2+} on the commercial γ-Al_2O_3 nanoparticles. $Ni(NO_3)_2{\cdot}6H_2O$ solution (8 ml, 0.1M) was added into the grinded γ-Al_2O_3 (0.0860g) and stirred at room temperature followed by 800 ^oC calcination an 700 ^oC hydrogen reduction.

Material Characterization

The crystallinity of the hierarchical samples were identified by a X-ray diffraction (XRD, Ultima IV, Rigaku, Japan) using a Cu Kα source (λ=1.542 Å), with a scan step of 0.02° and a scan range between 10° and 90°. The crystalline sizes of the Ni nanoparticles can be estimated using Scherrer equation. The morphologies of the hierarchical structure were investigated through a scanning electron microscopy (SEM, JSM7600F, JEOL, Japan) with an accelerating voltage of 15 kV. The particale size distribution and detailed microstructures of Ni nanoparticles were characterized by a conventional transmission electron microscope (TEM, Tecnai G2 spirit Biotwin, FEI, US) with an acceleration voltage of 120 kV and a high resolution TEM (HRTEM, JEM-2100F, JEOL, Japan) with an acceleration voltage of 200 kV.

XPS spectrometer (AXIS Ultra DLD, Kratos, Japan) was employed to determine the chemical binding energy and valence state of element Ni, Al and O in the calcined samples. The Fourier transform infrared spectroscopy (FTIR) spectrums of NOAO samples were recorded on a spectrometer (Nicolet 6700, ThermoFisher, US) using KBr pellets in the range of 4000-400 cm^{-1} region.

N_2 adsorption-desorption isotherm was performed at 77 K, with an Physisorption and Chemisorption Analyzer (Autosorb-iQ-C, Quantachrome, US) to calculate the surface areas and pore size distributions of the samples. The surface areas were calculated by the Brunauer-Emmett-Teller (BET) method, and the pore size distribution was calculated from the adsorption isotherm curves using density functional theory (DFT) method. Hydrogen temperature-programmed reduction (TPR) was also conducted on the Autosorb-IQ-C instrument with a thermal conductivity detector (TCD), and a gaseous mixture of H_2 and Ar (1/10, v/v) was fed into the reactor at a rate of 40 mL/min with the temperature increasing from the ambient temperature to 800 °C at a ramp of 10 °C/min.

Thermogravimetric-differential scanning calorimetry (TG-DSC) measurements of a NiAl-LDH precursor was conducted on a Thermo Gravimetric Analyzer (Pyris 1 TGA, PerkinElmer, US) in a temperature range of 30 °C to 900 °C at a heating rate of 20 °C/min in air flow.

Catalytic performance

The performances of the catalysts on dry reforming of methane were tested at atmospheric pressure in a fixed bed quartz reactor reactor (Fantai-4100, Fantai, China). Before catalysis reaction, 100 mg of the calcined NOAO catalyst was filled in the quartz tube reactor and reduced in situ at 700 °C for 2h in a

continuous flow of 5% H_2/Ar (20 ml/min). After reduction, The feed mixture (20% CH_4, 20% CO_2, 60% Ar) at a total flow rate of 20 mL/min was introduced to the reactor, corresponding to a space velocity of 80000 h^{-1}. The reaction was conducted at a temperature range of 500-750 °C and the products were analyzed by gas chromatography (GC7900, Tianmei, China).

Results and Discussion

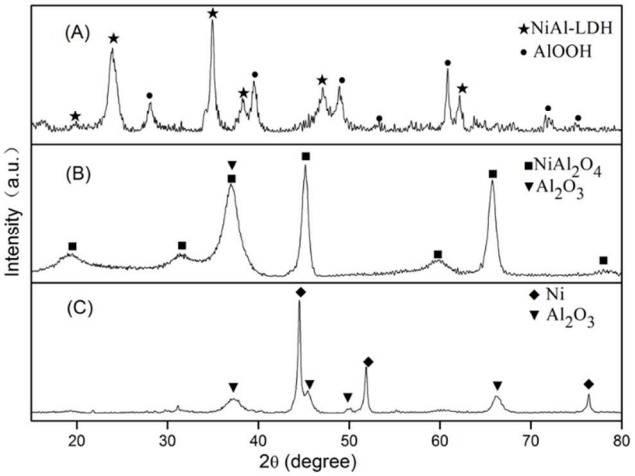

Figure 1. XRD patterns of the hierarchical Ni/Al_2O_3 composite prepared using a typical recipe with 8 ml of $Ni(NO_3)_2 \cdot 6H_2O$ (0.1 M), (A) as-obtained from hydrothermal treatment, (B) after calcination at 800 °C for 5 h, and (C) after H_2 reduction at 700 °C for 2 h.

The XRD patterns of the composite structures after hydrothermal reaction, calcination, and hydrogen reduction are displayed in Figure 1. The diffraction peaks of the samples after hydrothermal treatment (Figure 1A) can be indexed to the mixture of NiAl-LDH and AlOOH. The ratios of Ni/Al in LDH structure is normally between 1.5-4.[33] Therefore, we can easily adjust the Ni loading through changing the Ni/Al ratios. In our experiments, the Ni/Al ratio is less than 1, resulting in the presence of AlOOH phase. After calcination at 800 °C, no diffractions of NiO phase (2θ= 37.1°, 43.3°, and 63.1°) can be observed, suggesting that most of the Ni atoms enter the Al_2O_3 crystal lattice and form the $NiAl_2O_4$ spinel phase (2θ= 19.1°, 37.0°, 38.9°, 44.9°, 59.6° and 65.6°, Figure 1B). After reduction of the calcined sample at 700 °C, Ni nanoparticles were obtained, as shown in Figure 1C. Besides the XRD pattern of γ-Al_2O_3, the new peaks appearing at 44.7°, 52.1° and 76.6° can be indexed to the (111), (200) and (220) planes of the metallic Ni. According to the pioneer reports, the Ni/Al_2O_3 catalysts evolved from $NiAl_2O_4$ spinel phase usually have a strong interaction between the metal species and the support oxides, which can effectively limit the growth of Ni particles. A small size of metal particles can thus be expected. Based on the full width at half maximum (FWHM) of Ni (111) plane, the average size of the metal nanocrystals in NAO is 5.6 nm calculated by Scherrer's equation. In addition, the nitrogen adsorption/desorption isotherm of the hierarchical structure shows typical type IV curve with a hysteresis loop indicating a microporous-mesoporous structure, Figure S1A, B. The BET surface area of the composites is 177 m^2/g and mesopore size distribution exhibits a maximum centered at 3.5 nm.

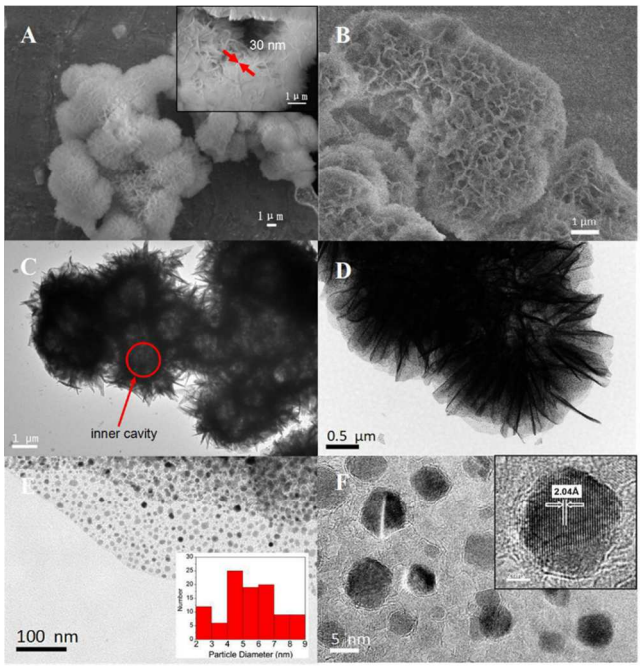

Figure 2. SEM images of hierarchical Ni/Al_2O_3 catalysts prepared in the typical synthesis route (A) before and (B) after calcination at 800 °C for 5 h. (C, D, E) The TEM image of hierarchical Ni/Al_2O_3 catalysts after H_2 reduction at 700 °C for 2 h with various magnifications. (F) HRTEM image of Ni nanoparticles.

The morphologies of hierarchical samples were characterized by SEM, TEM, and HRTEM techniques. The scanning electron microscopy (SEM) image (Figure 2A) shows that the as-synthesized LDH through hydrothermal reaction are 3D-hierarchical microspheres with highly rough outer surfaces and a diameter of 3-3.5 um. Higher magnification SEM image (Figure 2A, inset) further shows that the external surface of these hierarchical spheres is constructed by plenty of 2D-nanoflakes interconnected with each other. The thickness of the nanoflakes is ~ 30 nm. After calcination at 800 °C, no significant change on the morphology is observed. The mixed oxides, $NiAl_2O_4$ and Al_2O_3, preserved the hierarchical structure (Figure 2B). No apparent collapse of hierarchical spheres was observed, even though the particles have undergone 800 °C calcination for 5 h. This suggests a good structural stability and integrity of the nanocomposites, which is essential for applications in high temperature catalysis. The N_2 adsorption-desorption isotherms don't reflect the detailed information about macropores larger than 100 nm.[37] Nevertheless, from Figure 2B, we observe the main morphology of open slit-like pores with a diameter of 200-300 nm on the surface of microspheres. Such unique porous architecture may serve as ideal support, which not only provides interconnected open pores ensuring rapid diffusion of reactants and products, but also guarantees large surface areas providing more active sites for catalytic reaction.[2,38-39] Transmission electron microscopy (TEM) images (Figure 2C, D) reveal a typical porous hierarchical hollow spheres with flower-like shells constructed by nanoflakes. The diameter of the inner cavity is ~2-3 μm and the scale of the shell wall is ~300-400 nm. Small dark particles well dispersed on nanoflakes are observed in Figure 2D and 2E, which can be attributed to Ni nanoparticles. Figure 2E, F show the higher mag TEM images of the sample treated by hydrogen reduction. The dark stripes and the film-like region in Figure 2D can be indexed to the

projections taken along the edges and planes of nanoflakes, respectively. The thickness of the nanoflakes is approximately 36 nm through the evaluation from dark stripe, which is well consistent with the SEM observation. The Ni nanoparticles with a mean diameter of ~5.5 nm embedded on the surface of nanoflakes with rather high density are observed in Figure 2E and 2F. The slight particle size difference between XRD (~8 nm) and TEM result (av. 5.5 nm) may be caused by the defect-rich nature of the embedded particles.[40] A typical HRTEM image of the Ni particle is shown in Figure 2F .The lattice fringes present a lattice distance of 0.204 nm, corresponding to the (111) planes of pure Ni.

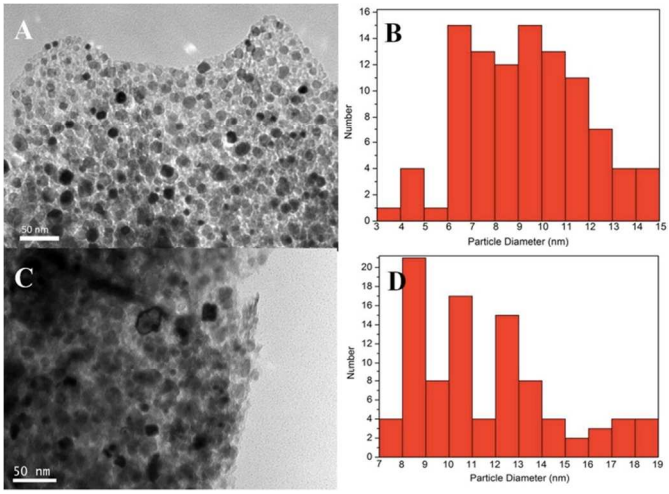

Figure 3. (A) TEM images of hierarchical Ni/Al_2O_3 catalysts with 47 wt% Ni loading and (B) its particle distribution; (C) TEM images of hierarchical Ni/Al_2O_3 catalysts with 58 wt% Ni loading and (D) its particle distribution.

The morphologies of the samples with various Ni loading are shown in Figure 3. The NAO (47 wt%, 800 °C) sample shows more concentrated particles than the typical one and the average size of Ni particles is ~10 nm (Figure 3A, B). With a higher Ni loading (Ni loading=58 wt%), a higher density of Ni particles with an average particle size of ~12 nm embedded on the flakes can be observed (Figure 3C, D). Even though several particles with the size of ~20 nm are observed, no severe sintering is observed during the annealing process, suggesting a strong sintering resistance of hierarchical Ni/Al_2O_3. However, nanoparticles with high surface area have an inherent tendency to minimize their energy through aggregation.[28] Obviously, the sample with higher Ni density has a larger tendency for Ni NPs to aggregate, especially under high temperature reactive environment, *e.g.* DRM reaction. An appropriate Ni/Al ratio should be thus selected.

Calcination temperature of the oxide precursors before hydrogen reduction is essentially important for the formation of spinel intermediate, which have strong effect on the Ni NPs and the metal-support interaction after H_2 reduction. We therefore investigated the effect of the calcination temperatures on the morphologies and the catalytic activities of the finally resulted samples. The catalysts that were annealed at 400 °C and 600 °C show metal particles >50 nm (Figure S2A, B) after 700 °C H_2 reduction. Many small pores are observed on the surface of Al_2O_3 matrix of the samples annealed at 400 °C and 600 °C. Besides the large particles, some small particles (< 10 nm) are also observed, as noted by the arrows in Figure S2A, B. The large Ni particles may be a result of the sintering of Ni NPs that were derived from the reduction of NiO and have loose contact with the support. During the sintering process, the loosely contacted Ni NPs would migrate on the surface of support, producing larger Ni particles and leaving pores on the original positions. The small nanoparticles (< 10 nm), however, are suspected to be derived from the reduction of $NiAl_2O_4$, which corresponds to a stronger metal-support interaction and therefore a limited mobility on the surface of the support and resistance to sintering. As a contrast, the sample that was calcined at 800 °C before H_2 reduction shows smaller metal particles (~ 5.5 nm, Figure 2D, E) due to the formation of mainly $NiAl_2O_4$ for Ni^{2+}, as proved by the XRD in Figure 1B.

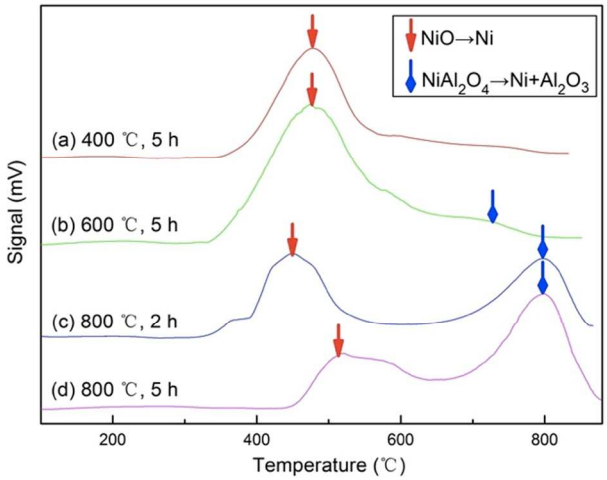

Figure 4. Temperature programmed reduction (TPR) curves of hierarchical NiO-γ-Al_2O_3 samples that were (a) calcined at 400 °C for 5 h , (b)calcined at 600 °C for 5 h, (c) calcined at 800 °C for 2 h, (d) calcined at 800 °C for 5 h.

The temperature programmed reduction (TPR) profiles of the samples annealed at various temperatures are shown in Figure 4. TPR is believed to reflect the energy bonds between the metal species and its environment.[39] Small NiO particles strongly bonded to the support is normally reduced at higher temperatures than large particles with poor metal-support interaction.[39-41] The samples annealed at 400 °C and 600 °C showed similar peak maxima around 450-500 °C, which can be ascribed to the weak contact between NiO and Al_2O_3 support (curve a, b in Figure 4). The XRD patterns confirm the presence of NiO in these two samples (Figure S3). The weak $NiAl_2O_4$ X-ray diffraction peak agrees with the weak TPR peak at 720 °C in the 600 °C calcined sample. Besides the reduction of NiO at 500 °C, strong TPR peaks at 800 °C are observed for the two samples annealed at 800 °C for 2 h and 5 h due to the formation of spinel phase. This result suggests that strong interaction between the resulted metal nanoparticles can be obtained only at high calcination temperatures that lead to the formation of spinel structures. Furthermore, the calcination time also plays a significant role in the interaction between metal and support. With calcination duration extended to 5 h at 800 °C, the low peak maxima shifted to a high temperature and the intensity ratio of I_{800} increased, which indicates a stronger interaction between metal and the support than the sample calcined at 800 °C for 2h (curve c, Figure 4). It seems that the full formation of spinel phase is slow, and enough time is required to obtain strong interactions between metal and the support.

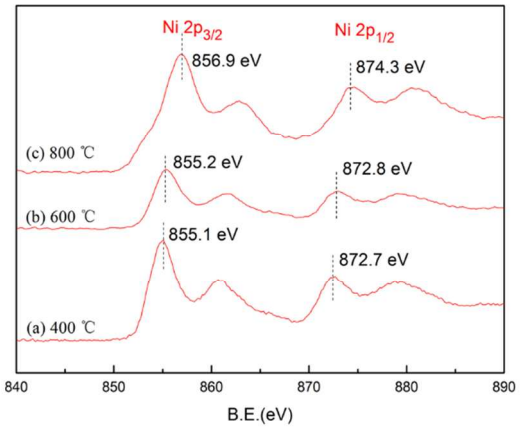

Figure 5. Ni XPS spectra of the hierarchical composite nanostructures calcined at (a) 400 °C, (b) 600 °C, and (c) 800 °C.

The XPS spectra were conducted to gain more details about the chemical states of the elements in the samples calcined at different temperatures and shown in Figure 5. With increasing calcination temperature, the binding energy of Ni $2p_{3/2}$ increases, suggesting increased bond strength between metal ions and the support. The Ni $2p_{3/2}$ binding energy of the sample annealed at 800 °C is around 856.9 eV. According to the previous reports, the binding energy of Ni $2p_{3/2}$ is ~ 853.6 eV in free NiO, 856.5 eV in NiO intimately contact with Al_2O_3 matrix, and 857.0 eV in the form of $NiAl_2O_4$.[39] The broad peak at 862- eV was assigned to the shakeup satellite peak. Based on the results of XPS and XRD, the Ni species in the sample annealed at 800 °C mainly exist in the form of $NiAl_2O_4$ spinel phase instead of free NiO. Compared with the sample annealed at 400 °C, the sample annealed at 600 °C shows a similar XPS value of 855.2 eV for Ni $2p_{3/2}$, which is consistent with the TPR results (Figure 5, curve a, b). In addition, their XRD results also confirm the existence of NiO instead of spinel phase (Figure S3). Therefore, the Ni species in the sample annealed at 400 °C and 600 °C should be mainly NiO weakly contacted with Al_2O_3 matrix. The XPS results also showed the relative quantity of Ni loading in the samples. Even though the Ni loading estimated from XPS analysis only reflects the surface atomic information and has deviation from the precursor Ni/Al ratios, the data in Table S1 still reflect the Ni loading change and are consistent with Ni amount in precursors.

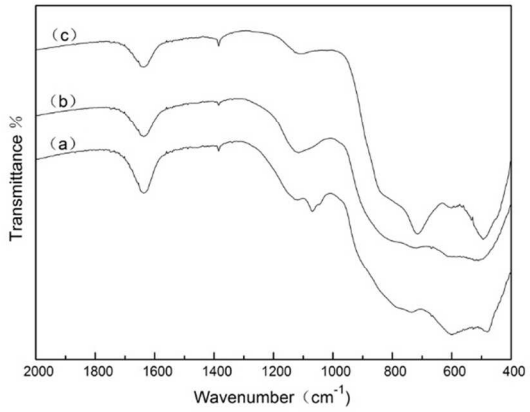

Figure 6. FTIR spectra of hierarchical Ni/Al_2O_3 catalyst calcined at (a) 400 °C, (b) 600 °C, and (c) 800 °C.

Figure 6 shows the FTIR profiles of the samples at various calcination temperatures. The FTIR further confirms the formation of Ni/Al_2O_3 after high temperature calcination. For the sample calcined at 800 °C, two obvious adsorption band at 740 cm^{-1} and 505 cm^{-1} are observed, which can be assigned to the stretching vibrations of the isolated tetrahedra (AlO_4) and average stretching vibration of (AlO_6) and (NiO_6) octahedra.[42-44] A small shoulder at 600 cm^{-1}, characteristic for $NiAl_2O_4$ structure, is also identified[43] In the case of samples calcined at lower temperatures, the absorption bands at 740 cm^{-1} and 505 cm^{-1} are broad. Unexpectedly, a shoulder at 600 cm^{-1}, characteristic for $NiAl_2O_4$ structure, was also identified. This suggests the local existence of spinel phase for the samples annealed at lower temperatures. The similar results were also observed by Jitianu.[44] They suggested the local order spinel phase can be attributed to the special decomposition mechanism for HT-like structures and the very good dispersion of cations in this kind of precursors.

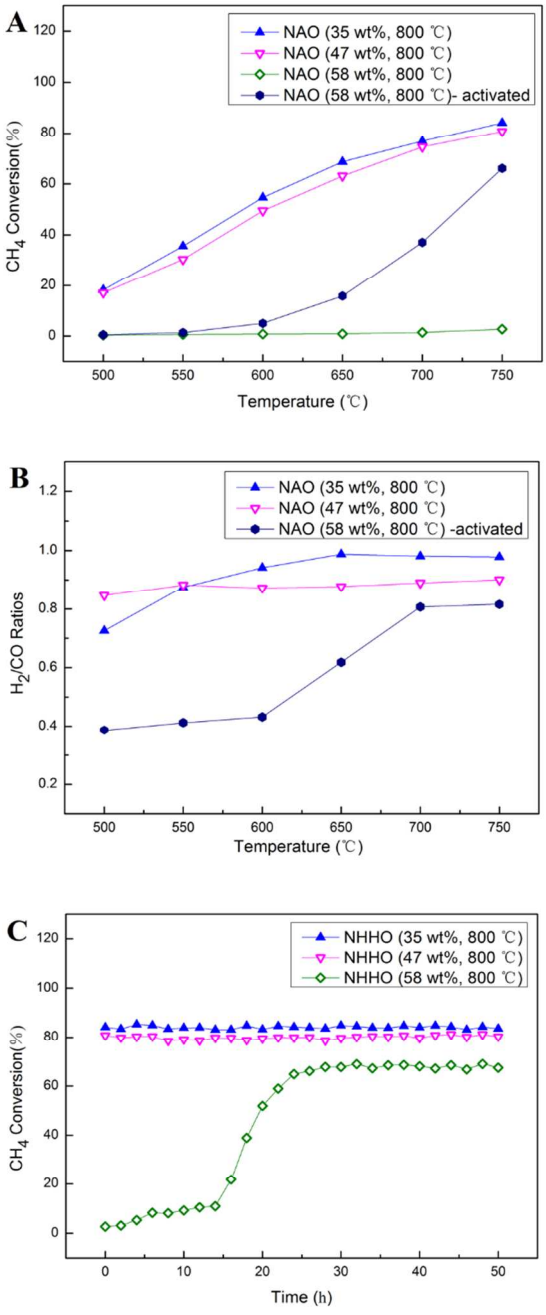

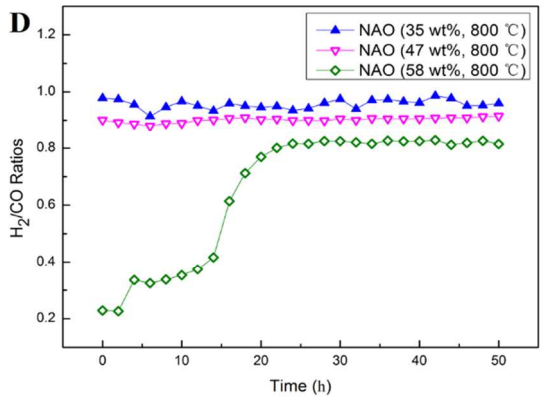

Figure 7. DRM catalysis of hierarchical Ni/Al_2O_3 catalysts with various Ni loadings. (A) Methane conversion of DRM catalysis, (B) H_2/CO ratio of the catalysis products, (C) Methane conversion and (D) H_2/CO ratio of DRM catalysis in a long term test (50 h) at 750 °C

The catalytic performances of the hierarchical Ni/γ-Al_2O_3 catalysts with different Ni loadings were characterized for DRM reaction. The methane conversion and H_2/CO ratios as a function of temperature in DRM catalysis are presented in Figure 7. All of the catalytic experiments were performed in a temperature range of 500-750 °C at a constant space velocity (80000 h^{-1}). The catalyst NAO (35 wt%, 800 °C) shows a little higher CH_4 conversion than NAO (47 wt%, 800 °C) at all the temperatures, which is very close to the equilibrium.[45] Both of them are much more active than NAO (58 wt%, 800 °C), which shows almost no catalytic activity in the initial tests. All of the samples show a H_2/CO less than 1 because of the accompanying reverse water-gas shift reaction (RWGS, $H_2+CO_2 \rightarrow H_2O+CO$), which produces H_2O and CO in DRM reaction.[46] NAO (35 wt%, 800 °C) shows the highest H_2 production, implying the best H_2 selectivity (Figure 7D). Since almost no catalytic activity for NAO (58 wt%, 800 °C) in the initial test is observed, H_2/CO ratio data for the sample is not shown in Figure 7B. However, the long term stability test shows an interesting phenomenon (Figure 7C). In the case of NAO (35 wt%, 800 °C) and NAO (47 wt%, 800 °C), no obvious degradation for CH_4 conversion and H_2/CO ratios is observed, suggesting excellent stability of the catalysts. This is in agreement with the similarity in the morphologies of the Ni NPs in Figure 2E and 3A. Since the CH_4 conversion of NAO (58 wt%, 800 °C) increases gradually from 0% to 67% after 25 h, an incubation stage seems to exist for the sample. To the best of our knowledge, it is the first time to report the incubation stage for Ni/Al_2O_3 catalysts. The catalytic performance of this sample after incubation is tested again as a function of temperature and plotted in Figure 7A. Even though the catalytic performance of NAO (58 wt%, 800 °C) is still much lower than those of NAO (35 wt%, 800 °C) and NAO (47 wt%, 800 °C), an obvious activity for DRM reaction can be observed. It was proposed that CO_2 will be adsorbed on the surface of the basic support and participate in catalytic reaction.[16,47] High density of Ni particles, which cover most of the matrix surface as shown in Figure 3C, heavily block the reactant gas to reach the surface of Al_2O_3 or probable adsorbed intermediate species. This interrupts the reaction process and significantly depresses the catalytic activity. When the high temperature reaction continues, the exposed surface area of Al_2O_3 support increases due to the sintering of metal particles (Figure S4), which is beneficial to the reaction process. The average particle size determined from the TEM images (Figure 3C, Figure S4) changed from 12 nm to 14 nm. Besides, the lower catalytic performance of NAO (58 wt%, 800 °C) than those of NAO (35 wt%, 800 °C) and NAO (47 wt%, 800 °C) no matter before or after the incubation period can be ascribed to the large average particle size.

Besides the loading amount of Ni specifies, the morphologies of the support and the synthetic methods also affect the catalytic performance of the catalysts. For the comparison, the control samples, Ni/hierarchical hollow Al_2O_3 synthesized by impregnation (IM-NAO) and Ni/Al_2O_3 nanosheet synthesized by hydrothermal method, were used for DRM reaction. Figure S5 shows TEM images of these two catalysts. Clear differences in morphology among the three catalysts can be observed. Despite the similarity in the hollow hierarchical nature of the alumina support of IM-NAO and NAO, the Ni nanoparticles in IM-NAO show serious aggregation and the average particle size is larger than 50 nm. This can be attributed to the weak interaction between the impregnated Ni species and the support. For Ni/Al_2O_3 nanosheet synthesized by hydrothermal method, the average particle size is 15 nm, and most of the particles are in the size range of 7 to 24 nm. The thickness of the sheets will not be thicker than 8 nm, assuming that the thickness of the sheets will not be larger than the size of the wrinkle edge (bold curves in Figure S5D). Some pores are observed on the surface of Ni/Al_2O_3 nanosheets due to the surface mobility and the sintering of the Ni NPs. The conversions of CH_4 and the H_2/CO ratios are shown in Figure S6. It can be seen that NAO showed superior catalytic performance and H_2 selectivity to the IM-NAO and the Ni/Al_2O_3 nanosheet. Since the three samples have the same Ni loading and have all been treated under 800 °C calcination, the superior catalytic activity of the hollow hierarchical NAO nanostructures to the others can be attributed to the combination of the strong metal-support interaction and the space configuration of the hierarchical nanostructures that facilitates the catalytic reactions. Besides, the IM-Ni/γ-Al_2O_3 was synthesized through impregnation method from commercial γ-nm Al_2O_3 (SA = 200 m^2/g). The IM-Ni/γ-Al_2O_3 exhibited a similar catalytic activity with the IM-NAO and was inferior to NAO (Figure S7). Considering the high price of the γ-nm Al_2O_3, the NAO has advantage in both catalytic activity and industry production cost.

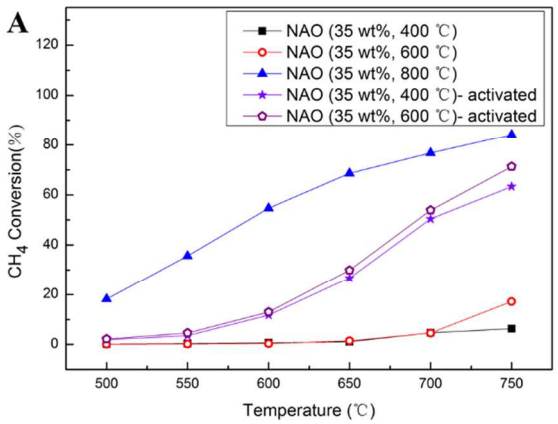

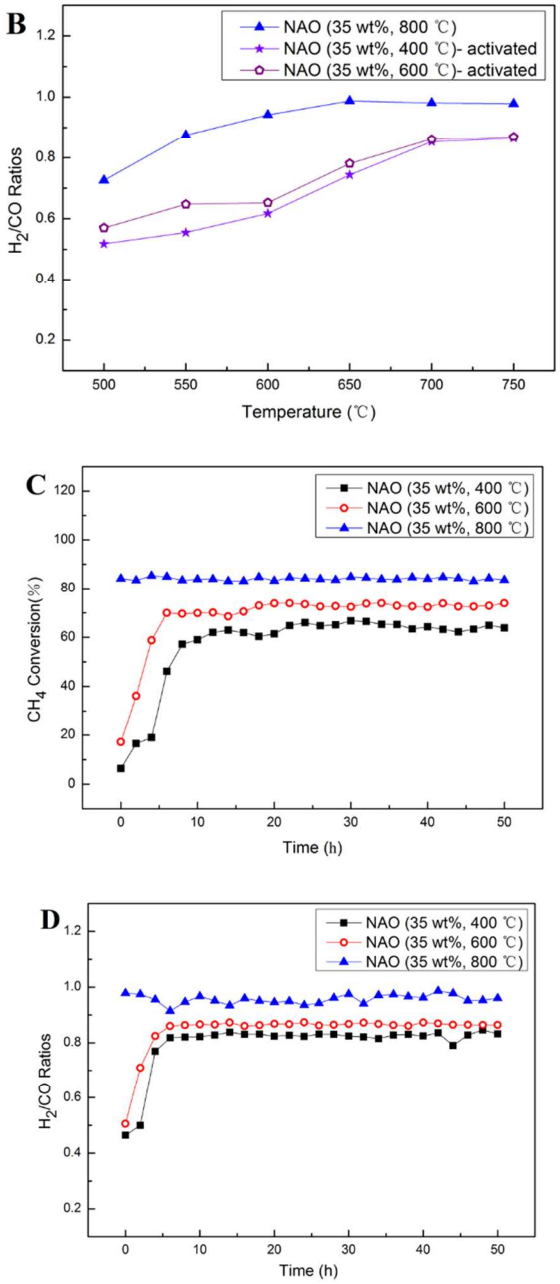

Figure 8. DRM catalysis of hierarchical Ni/Al_2O_3 catalysts (35 wt% Ni loading) with various calcination temperatures. (A) Methane conversion of DRM catalysis, (B) H_2/CO ratio of the catalysis products, (C) Methane conversion and (D) H_2/CO ratio of DRM catalysis in a long term test (50 h) at 750 °C

The calcination temperature plays a key role in the control over the particle sizes of the final Ni NPs, which are essential to the catalytic performances. The effects of the calcination temperatures were investigated on the samples with 35 wt% Ni loading. The H_2 reduced NAO (35 wt%, 400 °C) and NAO (35 wt%, 600 °C) show no activity for DRM reaction (Figure 8A). Interestingly, their catalytic activity improve gradually during the long term DRM reaction, as in the case of NAO (58 wt%, 800 °C). After that, these two samples show activities at the temperature range of 500-750 °C, Figure 8A, B. It should be noted that previous researches about Ni/Al_2O_3 catalysts for DRM reaction calcined at 600 °C didn't show the similar phenomenon.[28,39] The underling mechanism of these catalysts could be completely different from NAO (58 wt%, 800 °C), because these two samples have enough exposed Al_2O_3 surface. We believe the mechanism with respect to the phenomenon is related to two aspects, the interaction between metal and support and the surface -OH groups of the samples. As discussed in TEM and TPR results, the samples calcined at lower temperatures possess weaker interaction between the metal species and the oxide support. The metal particles are thus easy to migrate on the surface of the support and aggregate to form larger particles, which have less surface areas. Therefore, the mobility of the Ni particles limits the activity of the catalysts. The local spinel phase (described in FTIR results) possessing strong interaction between Ni species and support should have an influence on catalytic activity. However, the quantity of the spinel phase in the samples calcined at low temperatures is very little. The other aspect that might be the most crucial element for the catalytic performance may come from the surface hydroxyl groups. Ni *et al.* reported that the amount and chemical nature of -OH group play a significant role in the formation and successive decomposition of the intermediates in DRM reaction.[47] The basic -OH group is beneficial to the carbon suppress, whereas the strong acid -OH group will block the CO_2 adsorption on metal or support, resulting in poor catalytic activity. In our case, the decomposition of NiAl-LDH at relatively low calcination temperatures might result in a great amount of strong acid -OH group residue on the surface of metal and support, blocking the CO_2 and CH_4 adsorption.

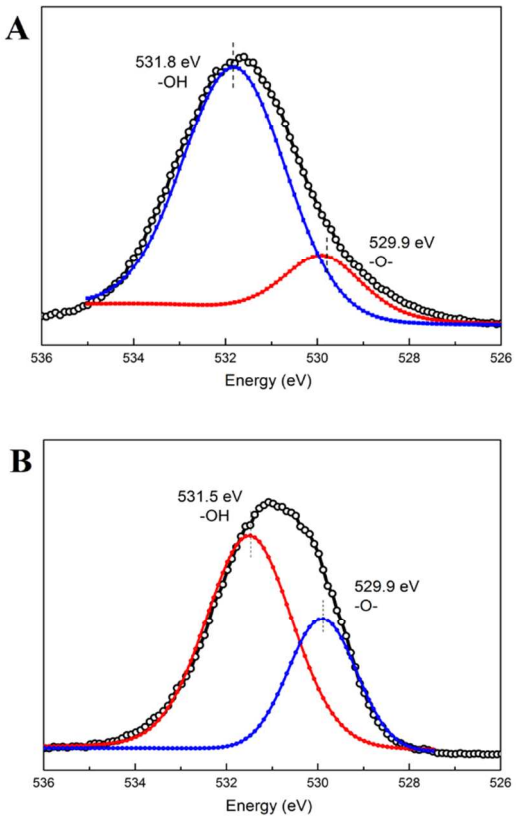

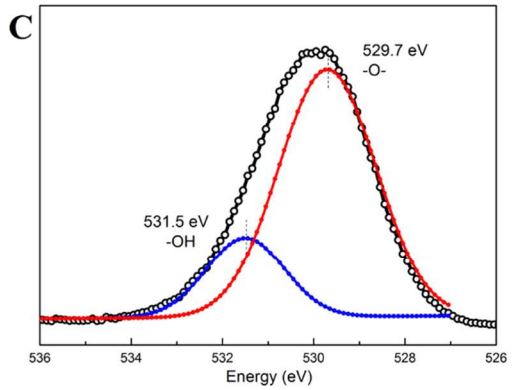

Figure 9. XPS of O1S for the samples calcined at various temperatures (A) 400 °C, (B) 600 °C, (C) 800 °C

The nature of the -OH groups is related to the calcination process. The thermal decomposition behavior by TGA analysis (Figure S8) shows almost 25% weight lost at 600 °C from the NiAl-LDH precursor. Although the calcination temperature of 800 °C can guarantee the decomposition of almost all the NiAl-LDH, there will still be some –OH residues. The O1s XPS spectra in Figure 9 confirms the existence of -OH groups on all the three samples. According to the pioneer results, the peak at 529.7 eV can be mainly attributed to the -O- in the type of metal oxides, while the peak at 531.5 eV is caused by the -OH group.[36] It is obvious that the -OH quantity reduces with the increase of calcination temperature. In the case of the sample calcined at 800 °C, the surface O1s is mainly from Al-O-Al instead of -OH groups and the peak area ratio of -OH/-O- is 0.3. On the contrary, the O1s peak at 531.6 eV indicates a high density of -OH groups on the surface of the sample calcined at 400 °C, where the -OH/-O- ratio is 4.2. The O1s peak of the sample calcined at 600 °C is the mixture of -OH and -O- and the ratio of -OH/-O- is 2.1. The calcination temperature therefore has a great effect on the nature of the catalyst surface. One probable mechanism is that the produced small amount of CO in the beginning react with surface -OH, leading to the formation of CO_2 via intermediate -COOH. This process gradually decreases the surface –OH groupds and thus activate the Ni/Al_2O_3 catalyst. Another mechanism would be the removal of chemical adsorbed -OH groups through H_2O and formation of oxygen vacancies on Al_2O_3 surface. Moreover, the incubation period for NAO (35 wt%, 600 °C) is 6 h, which is shorter than the 11 h of NAO (35 wt%, 400 °C). This result is rational due to the less -OH groups in NAO (35 wt%, 600 °C) than in NAO (35 wt%, 400 °C). Comparing with NAO (35 wt%, 400 °C), the interaction between metal and the support in NAO (35 wt%, 600 °C) shows an ignorable difference (see in TPR result, Figure 4). The CH_4 conversion for NAO (35 wt%, 400 °C) is lower than NAO (35 wt%, 600 °C). This may come from the residue of -OH groups in NAO (35 wt%, 400 °C), which can't be completely eliminated. Furthermore, the H_2 selectivity followed the order of Ni/Al_2O_3 (800 °C) > Ni/Al_2O_3 (600 °C) > Ni/Al_2O_3 (400 °C). This indicates a high calcination temperature is beneficial to the H_2 selectivity in DRM reaction.

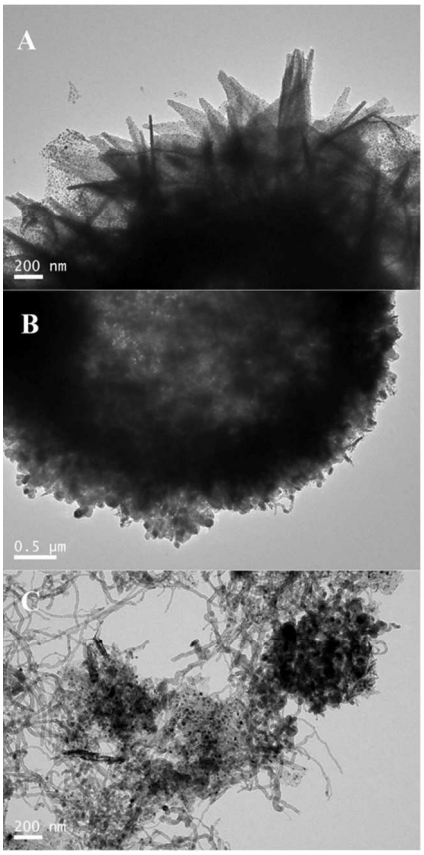

Figure 10. The TEM image of the spent (A)NAO (35 wt%, 800 °C), (B) IM-NAO (35 wt%, 800 °C) and (C) Ni/Al_2O_3 nanosheet (35 wt%, 800 °C) catalyst after long term test.

The NAO (35 wt%, 800 °C) shows the best catalytic performance among all the tested samples. The TEM image of spent catalyst and its particle size distribution are shown in Figure 10A and S9. No severe sintering of metal particles is observed for NAO catalyst after 50 h catalytic reaction. The average particle size determined from TEM analysis is 8.5 nm (Figure S9), a little larger than the ~5.5 nm of the fresh sample. In addition, no carbon whisker or nanotube can be detected. The average particle size determined from XRD analysis is 15 nm (Figure S10), and no peak of carbon is observed. Compared with the NAO, the IM-NAO and Ni/Al_2O_3 nanosheet produce obvious carbon filaments (Figure 10B, C). The carbon resistance therefore followed the order of NAO > IM-NAO > > Ni/Al_2O_3 nanosheet. It is worthy noticing that even though the average particle size in Ni/Al_2O_3 nanosheet is smaller than IM-NAO, the spent Ni/Al_2O_3 nanosheet shows much more carbon nanotubes. It seems that the hierarchical morphology can effectively limit the carbon deposition.

The observed superior catalytic performance of the sample calcined at 800 °C to the samples calcined at lower temperature is related to the strong interaction between metal and support and the large accessible surface area after hydrogen reduction. For the catalyst used in DRM reaction, the two main reasons for catalyst deactivation is the metal particle sintering and carbon deposition.[28,48] Generally, DRM reaction was usually carried out at 700 °C or above. Under this extreme condition, most of the metal particles usually aggregate and reduce active surfaces sites, which result in catalyst deactivation. The strong interaction between metal and support has a double effect, not only limits particle sintering, but also has a great effect on carbon deposition resistance. Recently,

Wang *et al.* claimed that if Ni particle was away from support surface, carbon species would encapsulate Ni particle by layer and block the active sites to contact with reactant gas, resulting in rapid catalyst deactivation.[49] Other researches also showed that small particles evolved from strong metal support interaction (SMSI) effect can effectively decrease the carbon deposition on the surface of metal particle[28,31]. Moreover, the large accessible surface area also plays a significant role. It has been reported that the carbon resource mainly comes from CH_4 decomposition (CH_4—C+2H_2). Meanwhile, the carbon elimination reaction (CO_2+C—2CO) can consume amorphous carbon rapidly.[46] The carbon amount would depend on the equilibrium of the above two reactions. Obviously, the large accessible surface area of NAO can effectively promote carbon elimination reaction from dynamic standpoint, which leads to a stronger carbon resistance.

Conclusions

In summary, we have prepared hollow hierarchical Ni/γ-Al_2O_3 nanostructured catalysts with γ-Al_2O_3 nanoflakes assembled on hollow Al_2O_3 spheres and well dispersed Ni nanoparticles embedded in Al_2O_3 nanoflakes. The Ni/γ-Al_2O_3 catalyst prepared through 800 °C calcination followed by hydrogen reduction shows a high surface area and a high loading (35 wt%) of metal particles, which demonstrates superior activities and stability during DRM catalysis to the control samples. The catalytic activities of the hierarchical Ni/Al_2O_3 in methane dry reforming reaction are closely related to the Ni loading and the precursor calcination temperatures that determine the formation of spinel $NiAl_2O_4$ intermediate. Reduction of spinel intermediate results in metal particles with smaller sizes and stronger metal-support interaction, which is crucial for the sintering and coke resistance properties of the catalysts. In the samples prepared with over loading of Ni and by lower precursor calcination temperature, initiate incubation is needed to activate the catalysts in DRM catalysis. This incubation process is proposed to be related to the sintering of over loaded Ni particles and the removal of the surface acidic -OH groups.

Acknowledgements

The authors greatly acknowledge the financial support by the National Natural Science Foundation of China (No.51172142), the Third Phase of 211 Project for Advanced Materials Science (No. WS3116205006 and WS3116205007), Shanghai Municipal Natural Science Foundation (No.12ZR1414300), and Starting Foundation for New Teacher of Shanghai Jiao Tong University (No.12X100040119).

Notes and references

1. State Key Lab of Metal Matrix Composites
School of Materials Science and Engineering
Shanghai Jiao Tong University
800 Dongchuan Rd.
Shanghai, P. R. China 200240
2. Key Laboratory of Polar Materials and Devices
Ministry of Education
East China Normal University, Shanghai, China

Electronic Supplementary Information (ESI) available: [details of any supplementary information available should be included here]. See DOI: 10.1039/b000000x/

1 W. Wang, S. Wang, X. Ma, J. Gong, *Chem. Soc. Rev.*, 2011, **40**, 3703.
2 J. Tian, H. Li, A. M. Asiri, A. O. Al-Youbi, X. Sun, *Small*, 2013, **9**, 2709.
3 J. Tollefson, *Nature*, 2009, **462**, 966.
4 S. N. Riduan, Y. Zhang, *Dalton Transactions*, 2010, **39**, 3347.
5 M.-S. Fan, A. Z. Abdullah, S. Bhatia, *ChemSusChem*, 2011, **4**, 1643.
6 N. A. S. Amin, T. C. Yaw, *Int. J. Hydrogen Energy*, 2007, **32**, 1789.
7 H. Y. Kim, J.-N. Park, G. Henkelman, J. M. Kim, *ChemSusChem*, 2012, **5**, 1474.
8 M.-S. Fan, A. Z. Abdullah, S. Bhatia, *ChemCatChem*, 2009, **1**, 192.
9 K. Wang, X. Li, S. Ji, B. Huang, C. Li, *ChemSusChem*, 2008, **1**, 527.
10 S. Wang, G. Q. M. Lu, *Appl. Catal. B: Environ.*, 1998, **16**, 269.
11 S. Zhang, S. Muratsugu, N. Ishiguro, M. Tada, *ACS Catal.*, 2013, **3**, 1855.
12 H. Xiao, Z. Liu, X. Zhou, K. Zhu, *Catal. Comm.*, 2013, **34**, 11.
13 J. Zhang, H. Wang, A. K. Dalai, *J. Catal.*, 2007, **249**, 300.
14 J. Zhu, X. Peng, L. Yao, D. Tong, C. Hu, *Catal. Sci. Technol.*, 2012, **2**, 529.
15 D. Baudouin, K. C. Szeto, P. Laurent, A. De Mallmann, B. Fenet, L. Veyre, U. Rodemerck, C. Coperet, C. Thieuleux, *J. Am. Chem. Soc.*, 2012, **134**, 20624.
16 X. Du, D. Zhang, L. Shi, R. Gao, J. Zhang, *J. Phys. Chem. C* ,2012, **116**, 10009.
17 N. A. Pechimuthu, K. K. Pant, S. C. Dhingra, *Ind. Eng. Chem. Res.*, 2007, **46**, 1731.
18 I. Luisetto, S. Tuti, E. Di Bartolomeo, *Int. J. Hydrogen Energy*, 2012, **37**, 15992.
19 Y. Zhao, S. Li, Y. Sun, *J. Phys. Chem. C*, 2013, **117**, 18936.
20 M. Souza, D. A. G. Aranda, M. Schmal, *Ind. Eng. Chem. Res.*, 2002, **41**, 4681.
21 S. M. Stagg-Williams, F. B. Noronha, G. Fendley, D. E. Resasco, *J. Catal.*, 2000, **194**, 240.
22 Y. G. Chen, K. Tomishige, K. Yokoyama, K. Fujimoto, *Appl. Catal. A-General*, 1997, **165**, 335.
23 K. Takanabe, K. Nagaoka, K. Aika, *Catal. Lett.*, 2005, **102**, 153-157.
24 M. Garcia-Dieguez, I. S. Pieta, M. C. Herrera, M. A. Larrubia, L. J. Alemany, *J. Catal.*, 2010, **270**, 136.
25 A. T. Ashcroft, A. K. Cheetham, M. L. H. Green, P. D. F. Vernon, *Nature*, 1991, **352**, 225.
26 W. Huang, K. C. Xie, J. P. Wang, Z. H. Gao, L. H. Yin, Q. M. Zhu, *J. Catal.*, 2001, **201**, 100-104.
27 L. L. Xu, H. L. Song, L. J. Chou, *Appl. Catal. B-Environ*, 2011, **108**, 177.
28 J. W. Han, C. Kim, J. S. Park, H. Lee, *ChemSusChem*, 2014, **7**, 451.
29 I. Lee, Q. Zhang, J. P. Ge, Y. D. Yin, F. Zaera, *Nano Res*, 2011, **4**, 115.
30 T. Xie, L. Shi, J. Zhang, D. Zhang, *Chem. Comm.*, 2014, **50**, 7250.
31 X. Du, D. Zhang, R. Gao, L. Huang, L. Shi, J. Zhang, *Chem. Comm.*, 2013, **49**, 6770.
32 H. Wang, X. Xiang, F. Li, *J. Mater. Chem.*, 2010, **20**, 3944.
33 G. Hu, N. Wang, D. O'Hare, J. Davis, *J. Mater. Chem.*, 2007, **17**, 2257.
34 X. Du, D. Zhang, L. Shi, R. Gao, J. Zhang, *Nanoscale*, 2013, **5**, 2659.
35 S. He, C. Li, H. Chen, D. Su, B. Zhang, X. Cao, B. Wang, M. Wei, D. G. Evans, X. Duan, *Chem. Mat*, 2013, **25**, 1040.
36 G. Chen, Y. Zhao, G. Fu, P. N. Duchesne, L. Gu, Y. Zheng, X. Weng, M. Chen, P. Zhang, C.-W. Pao, J.-F. Lee, N. Zheng, *Science*, 2014, **344**, 495.
37 L. Nie, A. Meng, J. Yu, M. Jaroniec, *Sci. Rep.*, 2013, **3**.
38 J. Wang, Z.-H. Hu, Y.-X. Miao, W.-C. Li, *Gold Bull.*, 2014, **47**, 95.
39 L. Xu, H. Song, L. Chou, *Appl. Catal. B-Environ*, 2011, **108**, 177.
40 K. Mette, S. Kuehl, H. Duedder, K. Kaehler, A. Tarasov, M. Muhler, M. Behrens, *Chemcatchem*, 2014, **6**, 100.
41 L. M. T. S. Rodrigues, R. B. Silva, M. G. C. Rocha, P. Bargiela, F. B. Noronha, S. T. Brandao, *Catal. Today*, 2012, **197**, 137.
42 F. Yongli, L. Wencong, Z. Liangmiao, B. Xinhua, Y. Baohua, l. Yong, S. Xingfu, *Cryst. Growth Des.*, 2008, **8**, 192.
43 H. W. Hou, Y. Xie, Q. Yang, Q. X. Guo, C. R. Tan, *Nanotechnology*, 2005, **16**, 741.
44 M. Jitianu, A. Jitianu, M. Zaharescu, D. Crisan, R. Marchidan, *Vib. Spectrosc.*, 2000, **24**, 307.
45 Z. Liu, J. Zhou, K. Cao, W. Yang, H. Gao, Y. Wang, H. Li, *Appl. Catal. B-Environ*, 2012, **125**, 324.
46 R. Shang, X. Guo, S. Mu, Y. Wang, G. Jin, H. Kosslick, A. Schulz, X.-

Y. Guo, *Int. J. Hydrogen Energy*, 2011, **36**, 4900.
47 J. Ni, L. Chen, J. Lin, S. Kawi, *Nano Energy*, 2012, **1**, 674.
48 W. Ning, Y. Xiaopeng, S. Kui, C. Wei, Q. Weizhong, *Int. J. Hydrogen Energy*, 2013, **38**, 9718.
49 N. Wang, K. Shen, X.Yu. *Catal. Sci. Tech.*, 2013, **3**, 2278.

Keywords

Ni/Al_2O_3, hierarchical, catalysts, hydrothermal, dry reforming of methane

Qing Zhang[1], Tao Wu[1], Peng Zhang[1]*, Ruijuan Qi[2], Rong Huang[2], Xuefeng Song[1], and Lian Gao[1]*

Title

Facile Synthesis of Hollow Hierarchical Ni/γ-Al_2O_3 Nanocomposites for Methane Dry Reforming Catalysis

ToC figure

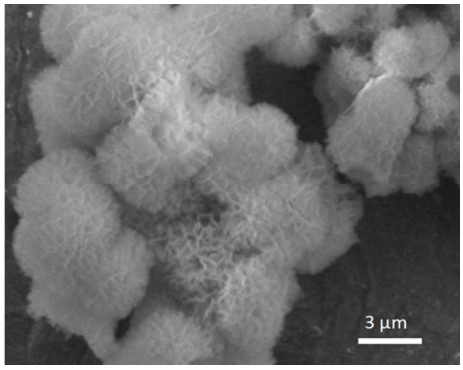

Hierarchical Ni/Al_2O_3 nanocomposite possesses a high surface area, high loading of well dispersed metal nanoparticles, and a hierarchical hollow structure. The strong interaction between metal and support and the large open accessible surface lead to excellent sintering and carbon resistance, and superior catalytic performance in methane dry reforming.